Thermal Conductivity

International Edition: DOI: 10.1002/anie.201511737
German Edition: DOI: 10.1002/ange.201511737

The Origin of Ultralow Thermal Conductivity in InTe: Lone-Pair-Induced Anharmonic Rattling

*Manoj K. Jana, Koushik Pal, Umesh V. Waghmare, and Kanishka Biswas**

Abstract: *Understanding the origin of intrinsically low thermal conductivity is fundamentally important to the development of high-performance thermoelectric materials, which can convert waste-heat into electricity. Herein, we report an ultralow lattice thermal conductivity (ca. 0.4 $W m^{-1} K^{-1}$) in mixed valent InTe (that is, $In^{+}In^{3+}Te_2$), which exhibits an intrinsic bonding asymmetry with coexistent covalent and ionic substructures. The phonon dispersion of InTe exhibits, along with low-energy flat branches, weak instabilities associated with the rattling vibrations of In^{+} atoms along the columnar ionic substructure. These weakly unstable phonons originate from the $5s^2$ lone pair of the In^{+} atom and are strongly anharmonic, which scatter the heat-carrying acoustic phonons through strong anharmonic phonon–phonon interactions, as evident in anomalously high mode Grüneisen parameters. A maximum thermoelectric figure of merit ($z T$) of about 0.9 is achieved at 600 K for the 0.3 mol% In-deficient sample, making InTe a promising material for mid-temperature thermoelectric applications.*

Thermoelectric materials can convert waste heat into useful electricity, and constitute a viable means to efficient energy management. The dimensionless figure of merit, $z T = S^2\sigma T/(\kappa_L + \kappa_e)$, determines their conversion efficiency and is derived from interdependent electrical conductivity (σ), Seebeck coefficient (S), and lattice (κ_L) and electronic (κ_e) thermal conductivities, where T is the temperature. The fundamental challenge in developing high-performance thermoelectric materials has been to achieve a simultaneous enhancement in power factor ($S^2\sigma$) and reduction in κ_L.[1] Significant reduction in κ_L of a material has been achieved through all-scale hierarchical architecting[2] and endotaxial nanostructuring.[3] On the other hand, intrinsically low κ_L originating in solids with complex crystal structures,[4] part-crystalline part-liquid state,[5] rattling modes,[6,7] soft phonon modes,[8] superionic substructure with liquid-like cation disordering,[9] resonant bonding,[10] and anisotropic layered crystal structure,[11] is of practical interest owing to its robustness against grain size and other structural variations.

[*] M. K. Jana, Dr. K. Biswas
New Chemistry Unit
Jawaharlal Nehru Centre for Advanced Scientific Research (JNCASR)
Jakkur P.O., Bangalore (India)
E-mail: kanishka@jncasr.ac.in
Homepage: http://www.jncasr.ac.in/kanishka/
K. Pal, Prof. Dr. U. V. Waghmare
Theoretical Sciences Unit
Jawaharlal Nehru Centre for Advanced Scientific Research (JNCASR)
Jakkur P.O., Bangalore 560 064 (India)

Supporting information for this article can be found under http://dx.doi.org/10.1002/anie.201511737.

Lattice anharmonicity and strong phonon–phonon interactions in specific materials can engender intrinsically low κ_L while preserving the carrier mobility.[12,13] The origin of lattice anharmonicity and the ensuing ultralow κ_L in the I-V-VI_2 chalcogenides, such as $AgSbSe_2$,[14] $AgBiSe_2$,[15] $AgBiS_2$,[16] and AgBiSeS,[17] has been traced to the electrostatic repulsion between the stereochemically active ns^2 lone pair of Group 15 cations and the valence p-orbital of Group 16 anions. Intrinsically low κ_L has also been evidenced in $Cu_{12}Sb_4S_{13}$[18] and $PbCuSbS_3$[19] due to the bond anharmonicity caused by stereochemically active $5s^2$ lone pair of Sb. The deformation of weak multicenter bonds in an electron-poor CdSb has been recently shown to cause lattice anharmonicity and thereby a low κ_L.[20] The concept of phonon glass electron crystal (PGEC) has been demonstrated earlier in some host–guest frameworks, as exemplified by clathrates[21] and filled skutterudites.[7,22] In these compounds, a guest atom rattles within oversized structural cages and scatters the heat-carrying acoustic phonons, thereby significantly lowering κ_L. The exploration of new materials with intrinsically low κ_L along with a microscopic understanding of the underlying correlations among bonding, lattice dynamics, and phonon transport is fundamentally important towards designing promising thermoelectric materials.

Herein, we report an ultralow lattice thermal conductivity ($\kappa_L \approx 0.4\ W m^{-1} K^{-1}$) in high-quality crystalline ingots of InTe, in a temperature range of 300–650 K. Using first-principles studies, we show the presence of strongly anharmonic phonons originating from rattling vibrations of In^{+} cations (along the z-axis) within the columnar ionic substructure, which couple with the heat-carrying acoustic modes and lead to an ultralow κ_L. By intentional p-type doping through creation of In-deficiencies, the power factor ($S^2\sigma$) can be enhanced to achieve a maximum $z T$ of about 0.9 at 600 K in the nominal $In_{0.997}Te$ sample, which is significantly higher than that of pristine InTe.

InTe, that is, $In^{+}In^{3+}Te_2$, is a mixed-valent compound belonging to tetragonal *I*4/*mcm* space group with a chain-type structure similar to TlSe.[23–25] The structure features coexistent ionic and covalent substructures. The In^{+} and In^{3+} cations are crystallographically inequivalent with distinct bonding environment. The trivalent In^{3+} cations form covalent (sp^3) In–Te bonds, which construct $In^{3+}Te_4^{2-}$ tetrahedra (Figure 1 a).[23,24] These tetrahedra share the horizontal edges to form covalently bonded anionic substructure with a chain-like topology along the crystallographic z-axis (Figure 1 a). The In^{3+}–Te bond distance of 2.81 Å is close to the sum of covalent radii of In (1.44 Å) and Te (1.35 Å).[23,24] On the other hand, each monovalent In^{+} cation is surrounded by eight Te atoms in a distorted square antiprismatic arrange-

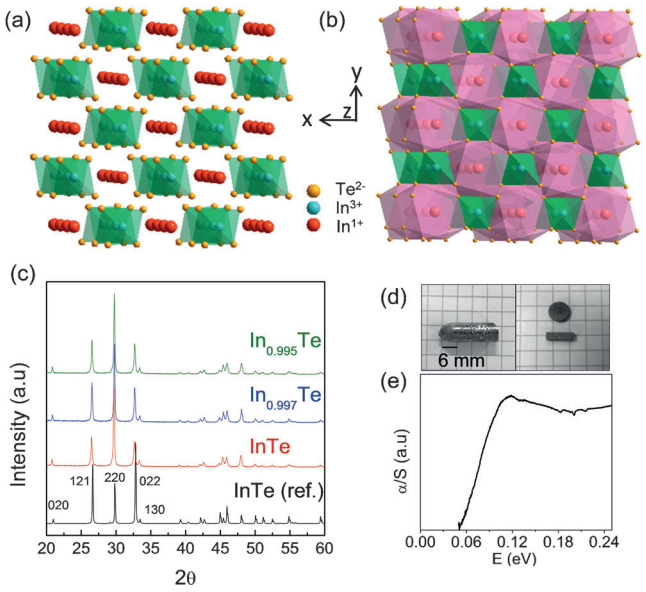

Figure 1. Crystal structure of InTe showing a) chains of covalently bound, edge-sharing $In^{3+}Te_4^{2-}$ tetrahedra (green) alternating with b) chains of face-sharing distorted Thompson cubes (pink) along the *z*-axis; c) powder XRD patterns of pristine InTe, $In_{0.997}Te$, and $In_{0.995}Te$ samples; d) bar and coin-shaped samples used for thermoelectric measurements; e) electronic absorption spectrum of InTe.

ment to form skewed Thompson cubes (Figure 1b).[23,24] These cubes share common square faces and form one-dimensional columnar ionic substructure along the *z*-axis (Figure 1b). The In^+–Te distance of 3.57 Å is close to the sum of ionic radii of In^+ (1.32 Å) and Te^{2-} (2.21 Å).[26] These chains of In^+ cations hold together the chains of $In^{3+}Te_4^{2-}$ tetrahedra by means of weak electrostatic interactions (Figure 1b). Along the chain direction (down the [001] axis), In^+–In^+ and In^{3+}–In^{3+} distances are 3.57 Å while the distance between In^+ and In^{3+} cations in the *a*-*b* plane is 4.23 Å.[23,24]

Crystalline ingots of pristine InTe and In_{1-x} Te ($x = 0.003$ or 0.005) were synthesized by melting the elements at 1073 K in evacuated quartz tubes (see the Supporting Information). The powder X-ray diffraction (PXRD) patterns of all the samples (Figure 1c) can be indexed on pure tetragonal InTe phase (*I*4/*mcm*). An optical band gap of about 0.06 eV was estimated for the pristine InTe, from diffuse reflectance spectroscopy (Figure 1e). The XPS In 3d spectra of InTe samples reveal an asymmetrically broadened doublet ($3d_{3/2}$ and $3d_{5/2}$), which can be deconvoluted into two pairs of Gaussian peaks separated by about 2 eV, corresponding to the In^+ and In^{3+} cations (Supporting Information, Figure S2).

Figure 2a shows the temperature-dependent (300–673 K) electrical conductivity (σ) of InTe and $In_{1-x}Te$ ($x = 0.003$, 0.005) samples, measured along the growth direction of the ingot. σ decreases with temperature for all the samples, which is characteristic of heavily doped (degenerate) semiconductors. Typically, for the pristine InTe, σ decreases from about 50 $S\,cm^{-1}$ at 300 K to about 18 $S\,cm^{-1}$ at 600 K. The value of σ near 300 K increases significantly to about 485 $S\,cm^{-1}$ for the In-deficient $In_{0.997}Te$ sample. For $In_{0.995}Te$, σ lowers to about 164 $S\,cm^{-1}$ at 300 K due to reduction in the carrier mobility (μ).

The room-temperature Hall coefficients (R_H) are positive for all the samples owing to dominant p-type conduction. The hole concentrations (n_H) at 300 K were determined by using the equation, $n_H = 1/e\,R_H$. n_H increases from about 5.8×10^{18} cm^{-3} in pristine InTe to about 2.8×10^{19} cm^{-3} and about 3.4×10^{20} cm^{-3} in $In_{0.997}Te$ and $In_{0.995}Te$ samples, respectively. Room-temperature carrier mobilities (μ) were determined using $\mu = \sigma/n_H e$. The value of μ increases from about 58 $cm^2\,V^{-1}\,s^{-1}$ in pristine InTe to about 108 $cm^2\,V^{-1}\,s^{-1}$ in $In_{0.997}Te$ sample and then drastically reduces to about 3 $cm^2\,V^{-1}\,s^{-1}$ in the $In_{0.995}Te$ sample.

Figure 2b shows the temperature-dependent Seebeck coefficient (S) of $In_{1-x}Te$ samples. S is positive for all of the samples due to p-type conduction. For the pristine InTe, S varies from about 211 $\mu V\,K^{-1}$ at 300 K to about 271 $\mu V\,K^{-1}$ at 608 K, peaking at a value of about 291 $\mu V\,K^{-1}$ at 560 K, which is suggestive of bipolar conduction owing to the narrow band gap of InTe. For the In-deficient samples, bipolar conduction is suppressed due to increased majority hole-carrier concentrations. The values of S near 300 K for nominal $In_{0.997}Te$ and

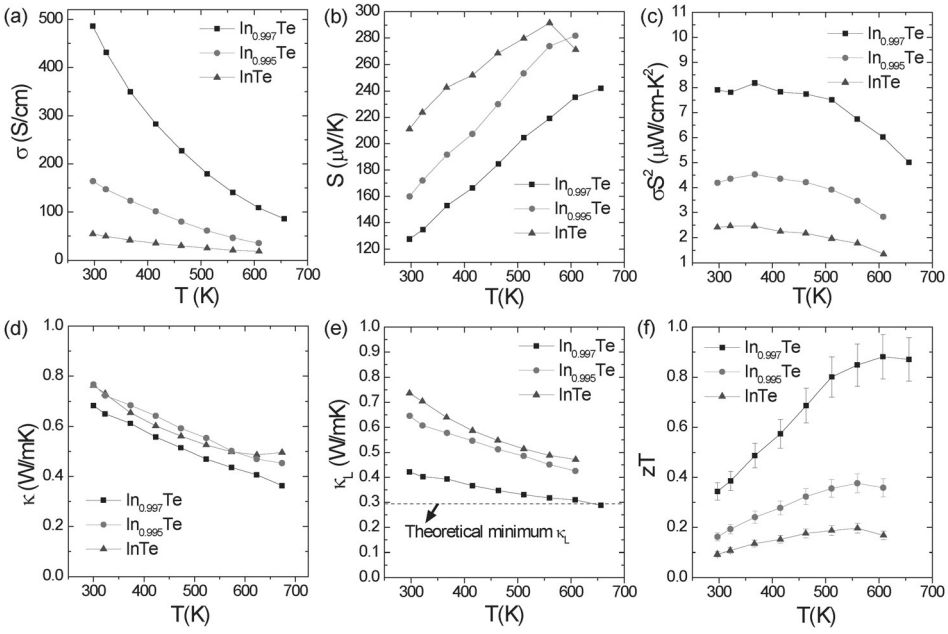

Figure 2. Temperature-dependent a) electrical conductivity (σ), b) Seebeck coefficient (S), c) power factor (σS^2), d) total thermal conductivity (κ), e) lattice thermal conductivity (κ_L), and f) thermoelectric figure of merit (zT) (with 10% error bars) of $In_{1-x}Te$ samples.

$In_{0.995}Te$ samples are about 127 $\mu V K^{-1}$ and about 159 $\mu V K^{-1}$, respectively.

The electron transport of pristine InTe and $In_{0.997}Te$ samples can be described using single parabolic band (SPB) model assuming the acoustic phonon scattering to be dominant (see the Supporting Information for SPB equations). The experimental S vs. n_H points lie on the theoretical Pisarenko plot generated using a density-of-states effective mass (m*) of $0.6\,m_e$ (Supporting Information, Figure S3). However the S versus n_H data point for $In_{0.995}Te$ sample deviates largely from the Pisarenko curve. The theoretically calculated electronic structure of InTe (Supporting Information, Figure S7) reveals two important features: a) two nearly degenerate valence band valleys at M- and Z-points, and b) the valence band at each of these points exhibits an inverted double well or "M"-shaped sub-valley structure. We speculate that high density p-type carriers resulting from heavy doping in $In_{0.995}Te$ ($n_H \approx 3.4\times10^{20}\,cm^{-3}$) populate the multiple valence bands, giving rise to a higher m^* and therefore an enhanced S in this sample.[14,27]

Figure 2c shows the temperature-dependent power factor ($S^2\sigma$) for all the samples. A maximum power factor of about 8 $\mu W cm^{-1} K^{-2}$ is obtained at 373 K for the $In_{0.997}Te$ sample, which maintains in excess of 5 $\mu W cm^{-1} K^{-2}$ up to 650 K. The high power factor in this sample is attributed to high carrier mobility and an optimized hole concentration.

Figure 2d shows the temperature-dependent total thermal conductivity (κ) of all the samples, measured along the ingot's growth direction. At 300 K, the pristine InTe exhibits a low κ value of about 0.76 $W m^{-1} K^{-1}$, which decays to about 0.5 $W m^{-1} K^{-1}$ at 673 K. For $In_{0.997}Te$ sample, κ varies from about 0.68 $W m^{-1} K^{-1}$ at 300 K to about 0.36 $W m^{-1} K^{-1}$ at 673 K. For $In_{0.995}Te$ sample, κ varies from about 0.76 $W m^{-1} K^{-1}$ at 300 K to about 0.45 $W m^{-1} K^{-1}$ at 673 K. To calculate lattice thermal conductivity ($\kappa_L = \kappa - \kappa_e$), the electronic thermal conductivity, κ_e, was extracted using Wiedemann–Franz law, $\kappa_e = L\sigma T$ where L is the temperature-dependent Lorentz number. For the pristine and $In_{0.997}Te$ samples, L was calculated using SPB model (see the Supporting Information for details), whereas a degenerate value of $L = 2.45\times10^{-8}\,W\Omega K^{-2}$ was used for the $In_{0.995}Te$ sample, given its high carrier density.

Figure 2e shows the κ_L of $In_{1-x}Te$ samples as a function of temperature. For all of the samples, κ_L follows T^{-1} dependence, indicating that the umklapp phonon–phonon scattering is dominant. For the pristine InTe, due to low electrical conductivity, κ_e is minimal and the total κ is dominated by κ_L, which varies from about 0.73 $W m^{-1} K^{-1}$ at 300 K to about 0.47 $W m^{-1} K^{-1}$ at 600 K. For the $In_{0.997}Te$ sample, κ_L at 300 K decreases to about 0.43 $W m^{-1} K^{-1}$, which further decays to as low as about 0.3 $W m^{-1} K^{-1}$ at 673 K. The reduction in κ_L with respect to the pristine InTe is expected to arise from phonon-scattering at the vacancies, which act as point defects. In principle, increased point defects in $In_{0.995}Te$ sample are expected to further lower κ_L value. However, κ_L of $In_{0.995}Te$ is higher than that of $In_{0.997}Te$. A heavily doped semiconductor ($n \approx 10^{20}\,cm^{-3}$) with multiple valence-band valleys coexistent at the Fermi level is known to show an interband carrier transfer, which causes an excess κ_e due to associated changes in energy.[28] The excess thermal conductivity during interband scattering cannot be accounted by the simple degenerate L value of $2.45\times10^{-8}\,W\Omega K^{-2}$, leading to an underestimation of the total κ_e as in the case of $In_{0.995}Te$. Thus, an increase of κ_L in $In_{0.995}Te$ ($n_H \approx 3.4\times10^{20}\,cm^{-3}$) compared to that in $In_{0.997}Te$ ($n_H \approx 2.8\times10^{19}\,cm^{-3}$) is probably due to an underestimation of κ_e in $In_{0.995}Te$ caused by interband carrier transfer. First-principles calculation of the electron–phonon interaction shows that two low-frequency phonon modes (ca. 21 cm^{-1} and 71 cm^{-1}) at wave vector $q = q_M - q_z$ strongly couple to the carriers, which indeed facilitate the interband scattering in InTe at a higher concentration of p-type carriers (see the Supporting Information for details). Such an interband scattering has been observed earlier in heavily p-type doped PbTe, where the κ_L value was larger than that of undoped PbTe due to an underestimation of κ_e caused by using the simple degenerate L.[29] The rapid decrease in μ for the $In_{0.995}Te$ sample does suggest an interband scattering of carriers that cause the anomaly in its calculated κ_L.

By using the calculated average sound velocities (Supporting Information, Table S1) of three acoustic modes, the minimum (amorphous limit) κ_L of InTe is estimated to be about 0.3 $W m^{-1} K^{-1}$ using the model developed by Cahill et al.[30] (see the Supporting Information for details) and is shown as a dashed line in Figure 2e. The experimental κ_L for the $In_{0.997}Te$ sample is remarkably low and decays to the amorphous limit of 0.3 $W m^{-1} K^{-1}$ at about 673 K. The low overall κ and κ_L values are highly desirable for thermoelectrics and are comparable to those of I-V-VI_2 chalcogenides, such as $AgSbSe_2$ and $AgBiS_2$, where the ns^2 lone pair of Group 15 cations causes a strong lattice anharmonicity and thereby a low κ_L.[12–14]

To uncover the precise origin of low κ_L, first-principles density functional calculations were carried out. Phonon dispersion of InTe calculated at its experimental lattice constant reveals a flat branch containing modes of imaginary frequencies (around $-16\,cm^{-1}$ at the Γ point) along Γ-X-M-Γ directions of the Brillouin zone (Figure 3a), which involve the displacement of only In^+ cations along z-direction (Figure 3c). Another branch containing an imaginary frequency ($-28\,cm^{-1}$) occurs at the Γ point, which involves antiparallel displacements of In^+ cations along the (±) z-direction and rotation of $In^{3+}Te_4^{2-}$ tetrahedra around z-axis through displacements of Te^{2-} anions in the xy-plane (Figure 3d). These unstable modes necessarily involve collective rattling vibrations of In^+ atoms (parallel to the z-axis) within the columnar ionic substructure. The region of these instabilities in the Brillouin zone implies that 1) rattling motion involves displacement of about six In^+ cations along the chain-direction, and 2) the In^+ displacements in adjacent chains are random. The thermally induced atomic displacement parameters (ADPs) of In^+ were indeed found to be significantly larger than those of In^{3+} and Te^{2-} and to be highly anisotropic with the maximum of vibration ellipsoid occurring in the z-direction towards the adjacent In^+ atoms ($U_{11} = U_{22} = 0.045\,Å^2$ and $U_{33} = 0.081\,Å^2$).[23] The large anisotropic ADPs indeed suggest In^+ atoms to behave as rattlers in InTe.

The total charge density of InTe at the experimental lattice constant (see Figure 4a) reveals strongly covalent In–

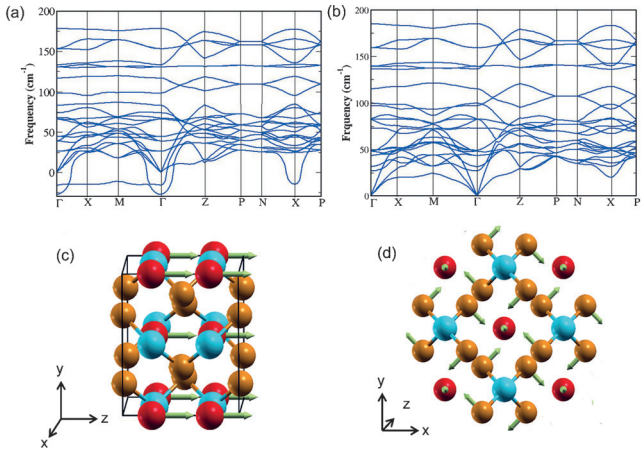

Figure 3. a) Phonon dispersion of InTe revealing two negative phonon branches with frequencies at −16 cm^{-1} and −28 cm^{-1} near the Γ point; the associated atomic vibrations are shown, respectively in (c) and (d) in the conventional tetragonal unit cell. Blue, red and yellow spheres denote In^{3+}, In^{+} and Te^{2-} atoms, respectively; b) Phonon dispersion of InTe at 3 GPa showing no negative frequency modes.

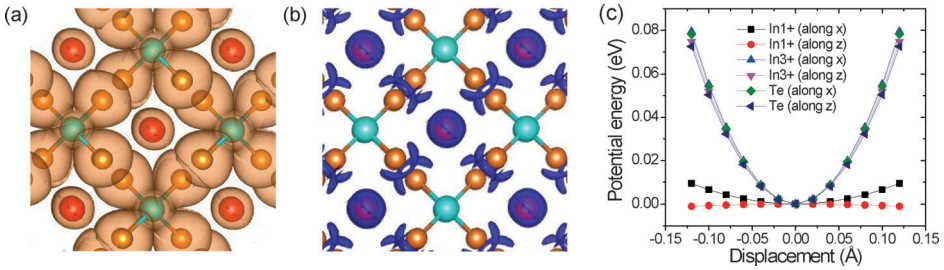

Figure 4. a) Isosurfaces of total charge density showing covalent bonding within the $In^{3+}Te_4^{2-}$ tetrahedron, and isolated In^{+} cations at the body center of the conventional tetragonal unit cell; b) ELF map (plotted at an iso-value of 0.88) reveals a nearly spherical charge density around In^{+} cation corresponding to its s^2 electron lone pair. Blue, red, and yellow spheres denote In^{3+}, In^{+}, and Te^{2-} atoms, respectively; c) calculated potential energy curves for all the atom types (In^{+}, In^{3+}, and Te^{2-}) as a function of displacement about the equilibrium positions, along *x*- and *z*-directions.

Te bonds within the $InTe_4^{2-}$ tetrahedron, as evident from its directionality between In^{3+} cation and the surrounding four Te^{2-} anions. Centrally inactive In^{+} cation is surrounded by a uniform spherical charge density arising from the $5s^2$ lone pair at the body center of the conventional tetragonal cell. To confirm the presence of a lone pair on the In^{+} cation, we examine the electron localization function (ELF) of InTe (Figure 4b). ELF measures the degree of electron localization in a molecule or a solid with information of local influence of the Pauli repulsion. The ELF analysis shows a spherical electron localization around In^{+} atoms, which is due to the $5s^2$ lone pair of In^{+}, and a lobe-shaped asymmetrically localized electron cloud around Te^{2-}, which constitutes the $5s^2$ lone pair of Te^{2-}, hybridized partially as permitted by its site symmetry. The spherical shape of a lone pair of an ion is known to cause its off-centering instability in a system.[31] Thus, the instabilities in the phonon spectrum originate from the $5s^2$ lone pair around In^{+} ions. On the other hand, the lobe-shaped lone pair on Te^{2-} ions causes their movement in the *xy*-plane (see Figure 3c) giving the rotational instability. By shifting the atoms away from equilibrium positions (along *x*- and *z*-directions), we find that the energy well of an off-centered In^{+} atom is very flat, unlike In^{3+} and Te^{2-} atoms, which sit in deep potential wells (Figure 4c). Thus In^{+} atoms are loosely bound to the lattice resulting in large ADPs. The energy of In^{+} displacements along *z*-axis is of shallow double well character.

The lattice thermal conductivity (κ_L) of a material is given by $1/3\,C_v v^2\tau$, where C_v, v, and τ are specific heat capacity, sound velocity, and relaxation time, respectively. Our calculations show that the frequencies of acoustic modes are less than 50 cm^{-1}, suggesting soft bonding in InTe. The zone center group velocities of acoustic branches, calculated along Γ-X, Γ-Z, and Γ-M directions (Supporting Information, Table S1) are very low, and hence their contribution to κ_L is weak. The ionic substructure with weakly bound In^{+} atoms results in anomalously large mode Grüneisen parameters (γ_i; Supporting Information, Table S1). Given the umklapp (U) and normal (N) phonon scattering rates are proportional to γ^2,[5] large values of γ_i reflect strong anharmonic phonon–phonon interactions in InTe.[13] Moreover the optical phonon instabilities ($\omega^2 < 0$) disappear in the phonon dispersion determined at a pressure of 3 GPa (see Figure 3b), showing that the rattling optical modes are strongly anharmonic, and can scatter the heat-carrying acoustic phonons through phonon–phonon interactions to effectively reduce τ and κ_L of InTe.

Figure 2f shows the temperature dependence of zT for all the samples. Indium deficiencies effectively increase power factor and give rise to a maximum zT of about 0.9 at 600 K in the nominal $In_{0.997}Te$ sample, which may be practically useful for mid-temperature thermoelectric applications.

In conclusion, InTe exhibits an ultralow lattice thermal conductivity approaching the theoretical minimum limit at elevated temperatures, which is attributed to the bonding asymmetry and lattice anharmonicity; In^{3+} cations covalently bond to Te atoms to form rigid substructure, whereas weakly bound In^{+} cations rattle along the ionic substructure, resulting in large thermally induced anisotropic ADPs. The collective rattling vibrations of In^{+} cations manifest as weakly localized branches with imaginary frequencies in the phonon dispersion; they are strongly anharmonic and scatter the heat-carrying acoustic phonons to effectively lower κ_L. The ionic substructure with rattling In^{+} atoms leads an intrinsically low κ_L, while the covalently bonded rigid substructure maintains the electrical conductivity, reflecting the phonon-glass electron-crystal nature of InTe. A maximum zT of about 0.9 is achieved at 600 K in the nominal $In_{0.997}Te$ sample, making InTe a promising material for mid-temperature thermoelectric applications.

Acknowledgements

This work was partially supported by DST Ramanujan Fellowship, Sheik Saqr Laboratory, and DAE-BRNS. U.V.W. acknowledges JC Bose National Fellowship, DST. We thank Prof. C. N. R. Rao for the fruitful discussion and continuous support. We thank Somnath Ghara for help with Hall measurements.

Keywords: indium telluride · lone pairs · rattling · thermoelectrics · ultralow thermal conductivity

How to cite: *Angew. Chem. Int. Ed.* **2016**, *55*, 7792–7796
Angew. Chem. **2016**, *128*, 7923–7927

[1] a) J. R. Sootsman, D. Y. Chung, M. G. Kanatzidis, *Angew. Chem. Int. Ed.* **2009**, *48*, 8616; *Angew. Chem.* **2009**, *121*, 8768; b) L.-D. Zhao, V. P. Dravid, M. G. Kanatzidis, *Energy Environ. Sci.* **2014**, *7*, 251.
[2] a) K. Biswas, J. He, I. D. Blum, C.-I. Wu, T. P. Hogan, D. N. Seidman, V. P. Dravid, M. G. Kanatzidis, *Nature* **2012**, *489*, 414; b) B. Poudel, Q. Hao, Y. Ma, Y. Lan, A. Minnich, B. Yu, X. Yan, D. Wang, A. Muto, D. Vashaee, X. Chen, J. Liu, M. S. Dresselhaus, G. Chen, Z. Ren, *Science* **2008**, *320*, 634.
[3] a) K. Biswas, J. He, Q. Zhang, G. Wang, C. Uher, V. P. Dravid, M. G. Kanatzidis, *Nat. Chem.* **2011**, *3*, 160; b) L.-D. Zhao, S. Hao, S.-H. Lo, C.-I. Wu, X. Zhou, Y. Lee, H. Li, K. Biswas, T. P. Hogan, C. Uher, C. Wolverton, V. P. Dravid, M. G. Kanatzidis, *J. Am. Chem. Soc.* **2013**, *135*, 7364.
[4] a) G. J. Snyder, E. S. Toberer, *Nat. Mater.* **2008**, *7*, 105; b) A. Zevalkink, E. S. Toberer, W. G. Zeier, E. Flage-Larsen, G. J. Snyder, *Energy Environ. Sci.* **2011**, *4*, 510.
[5] W. Qiu, L. Xi, P. Wei, X. Ke, J. Yang, W. Zhang, *Proc. Natl. Acad. Sci. USA* **2014**, *111*, 15031.
[6] a) H. Euchner, S. S. Pailhès, L. T. K. Nguyen, W. Assmus, F. Ritter, A. Haghighirad, Y. Grin, S. Paschen, M. de Boissieu, *Phys. Rev. B* **2012**, *86*, 224303; b) W. Schweika, R. P. Hermann, M. Prager, J. Perßon, V. Keppens, *Phys. Rev. Lett.* **2007**, *99*, 125501; c) D. J. Voneshen, K. Refson, E. Borissenko, M. Krisch, A. Bosak, A. Piovano, E. Cemal, M. Enderle, M. J. Gutmann, M. Hoesch, M. Roger, L. Gannon, A. T. Boothroyd, S. Uthayakumar, D. G. Porter, J. P. Goff, *Nat. Mater.* **2013**, *12*, 1028.
[7] X. Shi, J. Yang, J. R. Salvador, M. Chi, J. Y. Cho, H. Wang, S. Bai, J. Yang, W. Zhang, L. Chen, *J. Am. Chem. Soc.* **2011**, *133*, 7837.
[8] L. Bjerg, B. B. Iversen, G. K. H. Madsen, *Phys. Rev. B* **2014**, *89*, 024304.
[9] a) S. N. Guin, J. Pan, A. Bhowmik, D. Sanyal, U. V. Waghmare, K. Biswas, *J. Am. Chem. Soc.* **2014**, *136*, 12712; b) Y. He, T. Day, T. Zhang, H. Liu, X. Shi, L. Chen, G. J. Snyder, *Adv. Mater.* **2014**, *26*, 3974; c) H. Liu, X. Shi, F. Xu, L. Zhang, W. Zhang, L. Chen, Q. Li, C. Uher, T. Day, G. J. Snyder, *Nat. Mater.* **2012**, *11*, 422.
[10] S. Lee, K. Esfarjani, T. Luo, J. Zhou, Z. Tian, G. Chen, *Nat. Commun.* **2014**, *5*, 3525.
[11] L.-D. Zhao, S.-H. Lo, Y. Zhang, H. Sun, G. Tan, C. Uher, C. Wolverton, V. P. Dravid, M. G. Kanatzidis, *Nature* **2014**, *508*, 373.
[12] D. T. Morelli, V. Jovovic, J. P. Heremans, *Phys. Rev. Lett.* **2008**, *101*, 035901.
[13] M. D. Nielsen, V. Ozolins, J. P. Heremans, *Energy Environ. Sci.* **2013**, *6*, 570.
[14] S. N. Guin, A. Chatterjee, D. S. Negi, R. Datta, K. Biswas, *Energy Environ. Sci.* **2013**, *6*, 2603.
[15] a) S. N. Guin, V. Srihari, K. Biswas, *J. Mater. Chem. A* **2015**, *3*, 648; b) L. Pan, D. Bérardan, N. Dragoe, *J. Am. Chem. Soc.* **2013**, *135*, 4914; c) C. Xiao, X. Qin, J. Zhang, R. An, J. Xu, K. Li, B. Cao, J. Yang, B. Ye, Y. Xie, *J. Am. Chem. Soc.* **2012**, *134*, 18460.
[16] S. N. Guin, K. Biswas, *Chem. Mater.* **2013**, *25*, 3225.
[17] Y.-L. Pei, H. Wu, J. Sui, J. Li, D. Berardan, C. Barreteau, L. Pan, N. Dragoe, W.-S. Liu, J. He, L.-D. Zhao, *Energy Environ. Sci.* **2013**, *6*, 1750.
[18] W. Lai, Y. Wang, D. T. Morelli, X. Lu, *Adv. Funct. Mater.* **2015**, *25*, 3648.
[19] Y. Dong, A. R. Khabibullin, K. Wei, J. R. Salvador, G. S. Nolas, L. M. Woods, *ChemPhysChem* **2015**, *16*, 3264.
[20] S. Wang, J. Yang, L. Wu, P. Wei, J. Yang, W. Zhang, Y. Grin, *Chem. Mater.* **2015**, *27*, 1071.
[21] M. Beekman, G. S. Nolas, *J. Mater. Chem.* **2008**, *18*, 842.
[22] G. S. Nolas, D. T. Morelli, T. M. Tritt, *Annu. Rev. Mater. Sci.* **1999**, *29*, 89.
[23] J. H. C. Hogg, H. H. Sutherland, *Acta Crystallogr.* **1976**, *32*, 2689.
[24] A. M. Panich, *J. Phys. Condens. Matter* **2008**, *20*, 293202.
[25] Ş. Ellialtıoğlu, E. Mete, R. Shaltaf, K. Allakhverdiev, F. Gashimzade, M. Nizametdinova, G. Orudzhev, *Phys. Rev. B* **2004**, *70*, 195118.
[26] R. E. Jones, D. H. Templeton, *Acta Crystallogr.* **1955**, *8*, 847.
[27] Y. Pei, X. Shi, A. LaLonde, H. Wang, L. Chen, G. J. Snyder, *Nature* **2011**, *473*, 66.
[28] N. V. Kolomoets, *Sov. Phys. Solid State* **1966**, *8*, 799.
[29] J. Androulakis, I. Todorov, D.-Y. Chung, S. Ballikaya, G. Wang, C. Uher, M. Kanatzidis, *Phys. Rev. B* **2010**, *82*, 115209.
[30] D. G. Cahill, S. K. Watson, R. O. Pohl, *Phys. Rev. B* **1992**, *46*, 6131.
[31] R. Seshadri, N. A. Hill, *Chem. Mater.* **2001**, *13*, 2892.

Received: December 18, 2015
Revised: January 27, 2016
Published online: February 25, 2016

